Pan-STARRS Efficiency Notes

Pan-STARRS Internal Document

February 3, 2003

Abstract

We discuss various factors that impact Pan-STARRS efficiency.

Contents

List of Figures

Mauna Kea sky brightness measured by CFH12K

	B	V	R	I
Airmass = 1.0	22.3	21.4	20.8	19.6
Airmass = 1.5	22.1	21.0	20.5	19.4
Of. 50% moon	−1.2	−0.7	−0.3	−0.1

Table 1: in magnitude per square arcsecond

	B	V	R	I
Airmass = 1.0	1.5	4.5	7.8	18.0
Airmass = 1.5	1.7	6.2	10.0	21.3
Of. 50% moon	+3.1	+4.9	+2.5	+1.7

Table 2: in electrons per second per pixel for CCD09 (g=1.5 e−/sec)

Table 1: Measurements of sky brightness taken at CFHT.

List of Tables

1 Introduction

We discuss various factors that impact the performance of Pan-STARRS. Much of Pan-STARRS science will concern point sources, for which the performance is sensitive to the form of the point spread function (PSF). In §sec:efficiency:ptsrc we review the figures of merit for point source detection ($\propto A\Omega/\Delta\Omega$) and astrometry ($\propto A\Omega/(\Delta\Omega)^2$) where $\Delta\Omega$ is a measure of the area of the total system PSF. We discuss the, usually dominant, atmospheric seeing factor in the optical tranfer function. We then consider the effects of finite pixel size, charge diffusion, trailing losses, atmospheric refraction and telescope PSF, treating these, for the most part, as small perturbations. The approximation we use here is that convolution of the larger, quasi-Gaussian seeing disk with some more compact function simply causes an additative increase in the second moments. In §4 we explore the dependence of efficiency for asteroid detection on the filter pass-band. In §5 we discuss the limitation on astrometric precision imposed by the atmosphere. In §6 we describe the what the pipeline is supposed to deliver and how the performance of the image combination pipeline can be quantitatively assessed (though we make no attempt to do so).

2 Sky Brightness and Read-Noise

A weakness of multiple small telescopes as compared to a large telescope is that read-noise tends to be more important. Here we compute the loss of efficiency from finite read-noise as a function of exposure time and band-pass.

We will use measurements of the sky brightness taken at CFHT using the CFH12K and analysed by Jean-Charles Cuillandre. The results can be found at http://www.cfht.hawaii.edu/Instruments/Imaging/CFH12K/Optics.html and are reproduced in table 1.

	n_B	n_V	n_R	n_I
airmass=1	0.59	1.76	2.9	7.0
airmass=1.5	0.66	2.42	3.9	8.3
50% moon	+1.2	+1.9	+1.0	+0.66

Table 2: Number of electrons per pixel per second from the sky for Pan-STARRS.

	B	V	R	I	V+R	R+I
airmass=1	270	100	55	23	34	16
airmass=1.5	240	66	40	19	25	13

Table 3: Exposure times (in seconds) such that the effect of a 4 electron RMS read-noise causes a 10% reduction in efficiency (increase in observing time) as compared to a fictitious noise-less detector.

Assuming that the detector properties for Pan-STARRS as similar to CFH12K we can scale these results. Pan-STARRS will have $\simeq 30\%$ obscuration whereas CFHT has say $\simeq 15\%$. The primary diameter is 1.8M as compared to 3.6m. Pan-STARRS has an extra mirror (let's say 90% reflective). The pixel size for Pan-STARRS will be $\simeq 0''.3$ as compared to $\simeq 0''.207$ at CFHT. Putting all these factors together, the number of electrons per second per pixel will be the values given in the lower panel of table 1 times a factor

$$f = \frac{1.8^2}{3.6^2} \times \frac{1-0.3}{1-0.15} \times 0.9 \times \frac{0.3^2}{0.207^2} \simeq 0.39 \tag{1}$$

The resulting number of electrons per pixel per second from the sky n is given in table 2.

Read-noise will increase the noise in the image over that due to photon counting statistics. If the read-noise for a pixel has RMS value $\sigma_{\rm rn}$ electrons then, provided $\sigma_{\rm rn}^2 \ll nt_{\rm exp}$, the integration time required to reach a given signal-to-noise level increases, relative to a noise-less detector, by a factor

$$f = (1 + \sigma_{\rm rn}^2/nt). \tag{2}$$

This performance degradation is obviously greatest in dark-time. The goal for the Pan-STARRS detectors is to achieve a read noise of $\sigma_{\rm rn} = 2-3$ electrons. In table 3 we give the exposure times such that read-noise introduces a 10% overhead assuming, somewhat pessimistically, $\sigma_{\rm rn} = 4$. The last two columns show the necessary exposure times for non-standard filters as may be desired for e.g. detection of asteroids.

3 Point-Sources

The likelihood of a point source (a function of the flux density and position) can be computed from the summed image. The likelihood maxima reside at the peaks of a readily computable significance function $\nu(\mathbf{r})$. The fractional uncertainty in the flux density is $\Delta S/S = 1/\nu$ so nu is the signal-to-noise ratio. For an object which, on average delivers N electrons per second, the squared signal to noise is

$$\nu^2 = \frac{N^2 t_{\rm exp}}{\overline{n}} \int \frac{d^2k}{(2\pi)^2} |\tilde{g}(\mathbf{k})|^2 \tag{3}$$

where $\overline{n}$ is the electron count per unit solid angle from the sky (we are neglecting read- and digitization-noise here) and $\tilde{g}(\mathbf{k})$ is the system optical transfer function (i.e. the product of atmosphere, telescope and detector OTFs). More generally, $\tilde{g}^2(\mathbf{k})$ here is a sum of components from the various images weighted inversely by the noise variance.

The figure of merit for point source detection is therefore proportional to the zeroth moment of the OTF squared, or equivalently the integral $\int d^2r\ g^2(\mathbf{r})$ where $g(\mathbf{r})$ is the normalised PSF.

The uncertainty in the position (per component) is given by

$$\sigma_x^2 = \frac{1}{\nu^2} \frac{\int d^2g\ |\tilde{g}(\mathbf{k})|^2}{\int d^2g\ k_x^2 |\tilde{g}(\mathbf{k})|^2} \tag{4}$$

	B	V	R	I
μ	22.3	21.4	20.8	19.6
m_1	24.3	24.6	24.5	24.3
$m_{5/60}$	24.5	24.2	23.8	23.1

Table 4: Sky brightness μ; the magnitude of one square arcsecond of sky. Magnitude m_1 of a source that would generate one electron per second in a single telescope. The quantity $m_{5/60}$ is the magnitude of a point source that can be detected at the 5-sigma level in a 60 second integration using all four telescopes.

so the figure of merit for astrometry is proportional to the ratio of the second and zeroth moments of the OTF squared.

The total system OTF can readily be calculated for all of the components, and the dependence of the figures of merit on the various design parameters can be determined numerically. For Pan-STARRS, the dominant attenuating factor in the OTF comes from atmospheric seeing. If we model the atmospheric PSF as a 2-dimensional Gaussian, then including the other factors perturbatively results in an ellipsoidal PSF $g(\mathbf{r}) = \exp(-(x^2/\sigma_x^2 + y^2/\sigma_y^2)/2)$ where the dispersions σ_x^2 and σ_y^2 are the sum of the various components. The detection figure of merit, the inverse area of the total PSF, is then proportional to $1/(\sigma_x\sigma_y)$. In this way we can explore how the system performance (for detection at least) is controlled by the design parameters.

3.1 Atmospheric Seeing

This is well described by Kolmogorov theory, and numerical calculation gives the significance, in terms of the width of the seeing disk FWHM,

$$\nu^2 = 0.318 \frac{N^2 t_{\rm exp}}{\overline{n}({\rm FWHM})^2}. \tag{5}$$

For the commonly used Gaussian model for the PSF $g(\mathbf{r}) = \exp(-r^2/2\sigma^2)$ with $\sigma \simeq {\rm FWHM}/2.35$

$$\nu^2 = \frac{2\ln 2}{\pi} \frac{N^2 t_{\rm exp}}{\overline{n}({\rm FWHM})^2} \simeq 0.441 \frac{N^2 t_{\rm exp}}{\overline{n}({\rm FWHM})^2}. \tag{6}$$

The Gaussian model therefore underestimates the integration time required to reach a given signal-to-noise by about 40%. If m_1 is the magnitude of a source which delivers 1 electron per second, and μ is the magnitude of one square arc second of sky, then the Gaussian model gives the signal-to-noise as

$$\frac{\rm S}{\rm N} = \nu = \sqrt{\frac{2\ln 2}{\pi}} \frac{t_{\rm exp}^{1/2}}{\rm FWHM} 10^{0.2(m_1 - 2m + \mu)}. \tag{7}$$

Amusingly, a very good approximation to the correct Kolmogorov result is obtained if one drops the factor $2\ln 2$, and many of the science proposals use this model. Table 4 contains μ, m_1 and $m_{5/60}$, the limiting magnitude for a 5-sigma detection in a 60 second integration, all calculated from the CFHT observations.

If we specify the FWHM, then, in terms of area, the seeing disk is equivalent to a Gaussian of scale length

$$\sigma = \sqrt{\frac{0.441}{0.318}} \frac{\rm FWHM}{2.35} \simeq \frac{\rm FWHM}{2.0} \tag{8}$$

and we adopt this approximation below.

3.2 Finite Pixel Size

The finite extent of real pixels modifies the above results in two ways:

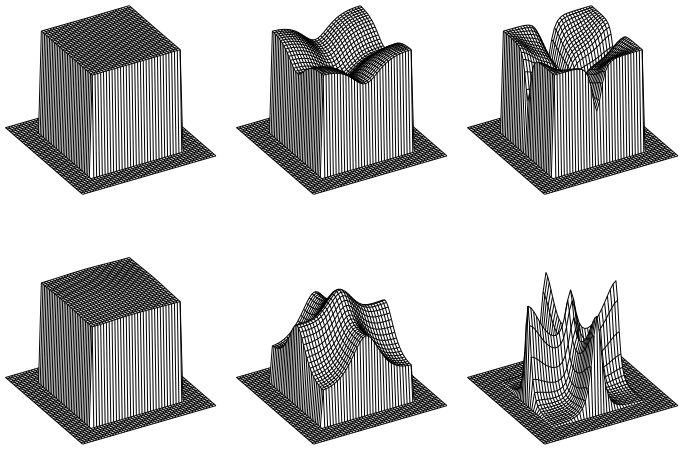

Figure 1: The top panels show the variation of the variance in source flux density with position for a simple model of a Gaussian PSF with scale length σ and square pixel of size d. The bottom panels show the variation of the position variance. As expected, these show that the flux density is best determined if the source lies at the center of a pixel which the position variance is lowest when the source lies at the pixel corner. From left to right, these show the variation for $d_{rmpix}/\sigma = 1.175,\ 2.35,\ 4.7$ respectively. For expected median seeing with FWHM = $0''.6$, corresponding to $\sigma \simeq 0''.3$, these correspond to pixel sizes of $0''.35$, $0''.7$ and $1''.4$. Clearly, for median seeing, and for pixel size of say $0''.3$, the variation of the variances is negligible. The central panel would then correspond to seeing with FWHM = $0''.26$.

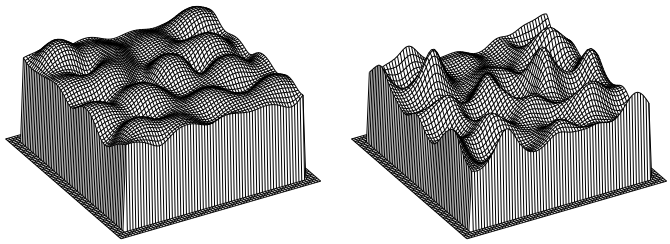

Figure 2: Variation of the flux density variance (left) and position variance (right) for the sum of four images with random shifts and rotations. The area shown is that of 16 pixels. The pixel size here is 2.35 times the Gaussian PSF scale length (i.e. like the central panels in figure 1). This would be the variation of sensitivity in exceptional seeing conditions.

1. It causes the squared significance ν^2 and position variance σ_x^2 to vary with the position of the source location relative to the pixel center; equations (3) and (4) are really averages over source location.

2. It increases the width of the PSF, decreasing the efficiency.

The magnitude of the first effect is illustrated in figure 1. These demonstrate that for a pixel size of $d_{\rm pix} \sim 0''.3$, and for typical seeing the effect is very small even for a single image. However, if Pan-STARRS makes simultaneous images this will reduce the variation of sensitivity still further, as shown in figure 2

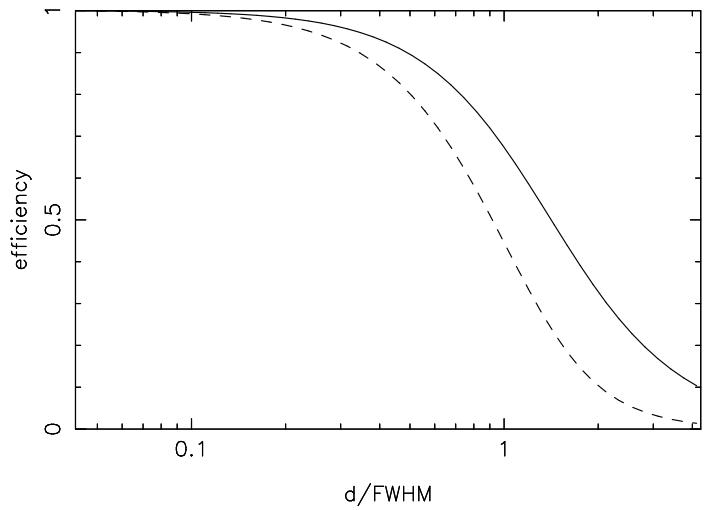

Figure 3: Numerical calculation of the effect of finite pixel size in the non-perturbative regime.

For any plausible seeing conditions, the main effect of finite pixel size is to increase the area of the PSF. Modelling the other components of the PSF as a Gaussian of width $\sigma = \mathrm{FWHM}/2.0$, the area of the PSF increases by a factor

$$\frac{\sigma^2 + d_{\mathrm{pix}}^{-1} \int_{-d\mathrm{pix}/2}^{d\mathrm{pix}/2} dx\, x^2}{\sigma^2} = 1 + \frac{d\mathrm{pix}^2}{12\sigma^2} \simeq 1 + \frac{d\mathrm{pix}^2}{3\mathrm{FWHM}^2} \tag{9}$$

which should be valid provided $d^2 \ll 3\mathrm{FWHM}^2$. For $d_{\mathrm{pix}} = 0''.3$ and $\mathrm{FWHM} = 0''.6$, the finite pixel size increases the PSF area by about 8%. In exceptional seeing conditions ($\mathrm{FWHM} = 0''.3$) the performance degrades by about 30%. The variation of performance in this regime is shown in figure 3.

3.3 Charge Diffusion

The effect of charge diffusion in the detector is to introduce a Gaussian blurring. The size of the Gaussian depends on wavelength and on the details of the detectors. Measurments at Lick suggest that a diffusion scale of $\sigma_{\mathrm{diff}} \sim 5\mu$m may be obtainable (it is very unlikely to be better than this). With a plate-scale of 40μm/arcsec (i.e. 12μm pixels with $d_{\mathrm{pix}} = 0''.3$) this corresponds to an angular scale of $\sigma_{\mathrm{diff}} \simeq 0''.125$. For $0''.6$ seeing this would give a degradation of performance of anout 17%.

The effect of charge diffusion is therefore likely to be much larger than the effect of finite pixel size, and is a critical factor in the system performance. Obtaining a small charge diffusion scale is a very high priority for the detector team.

3.4 Trailing Losses

The purpose here is to calculate the loss in efficiency for detecting point sources caused by their motion.

In principle, an optimal search for trailed objects would involve convolving the image with a series of templates, each of which is the convolution of the PSF with a line of length l and orientation ϕ and locate peaks, as a function of the four parameters l, ϕ and the 2 components of the center of the object. However, this is computationally expensive, especially for long arcs. A cheaper, though less efficient, alternative is to convolve with a matched filter that is the convolution of the PSF and the average of a line taken over all possible orientations.

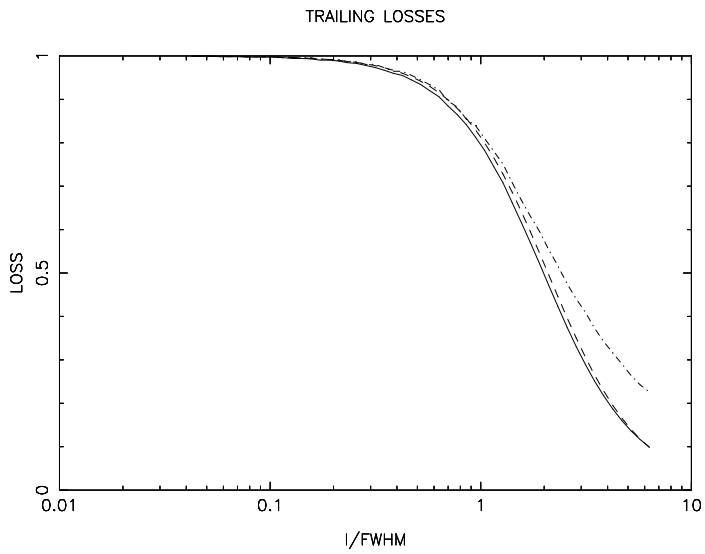

Figure 4: The solid line is the loss in efficiency for detection of moving sources as a function of the distance travelled l. This assumes a matched filter search for an object of known length but unknown orientation. The dash-dot line is the same for an object of known length and orientation. The dashed line is the simple model $1/(1 + l^2/24\sigma^2)$. A Gaussian system PSF was assumed for simplicity.

If one defines the efficiency ϵ as being proportional to the inverse of the time required to detect the object, then the efficiency is proportional to the integral

$$\epsilon \propto A \int d^2x \; g^2(\mathbf{x}) \tag{10}$$

where A is the collecting area and $g(\mathbf{x})$ is the PSF. Equivalently, since we normalise the PSF so that $\int d^2x \; g(\mathbf{x}) = 1$, the efficiency is the average of the PSF, or again equivalently, inversely proportional to the effective area of the PSF.

This definition of the efficiency is somewhat questionable, since, if we compare two systems with the same efficiency, but with different PSF widths and with compensatingly different collecting areas then the false detection rate will be lower for the system with the broader PSF. However, for reasonably secure detections (say 5-sigma or better), this is a relatively minor correction.

If the trail length is l, and the instrumental PSF $g_0(\mathbf{x})$, then the efficiency ratio is

$$R = \frac{\int d^2x \; g_0^2(\mathbf{x})}{\int d^2x \; g_l^2(\mathbf{x})} \tag{11}$$

where $g_l(\mathbf{x})$ is the convolution of $g_0(\mathbf{x})$ with the azimuthal average of a line of length l. The latter is proportional to $1/x$ for $x < l/2$ and is zero otherwise.

Figure 4 shows the trailing loss computed for a Gaussian system PSF model. The computed trailing loss is well described by the simple formula $1/(1 + l^2/24\sigma^2)$.

3.5 Atmospheric Refraction

Variation of the atmospheric refraction with wavelength will disperse images. The refraction curve from the CFHT Observer's Manual is shown in figure 5.

This is important for detection of hazardous asteroids. Efficient detection dictates a filter with a broad pass-band, but the objects are also most efficiently detected in the 'sweet-spots' that can only be observed at fairly high air-mass.

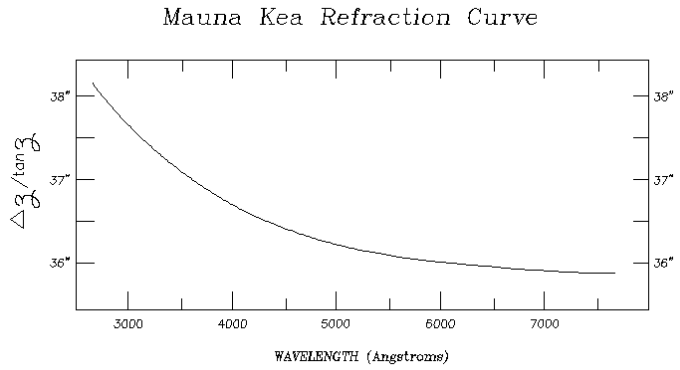

Figure 5: Refraction curve from the CFHT Observer's Manual. This differs noticeably from the formulae given by Allen. In particular, the slope at long wavelengths is lower than Allen gives, so the dispersion for long wavelengths is lower. We do not understand the cause of this discrepancy.

$\lambda_{\rm min}$	$\sigma^2_{\rm ref}(z=45^\circ)$	$\sigma^2_{\rm ref}(z=70^\circ)$
5500	4.91×10^{-3}	3.71×10^{-2}
5000	1.01×10^{-2}	7.62×10^{-2}
4500	2.03×10^{-2}	1.53×10^{-1}
4000	3.73×10^{-2}	2.81×10^{-1}

Table 5: Dispersion of images from differential atmospheric refraction.

The refraction, as a function of wavelength and zenith distance is $R(\lambda,z)=R_0(\lambda)\tan z$. If the number of electrons being created from the illumination from the source in the interval of wavelength $d\lambda$ is $n_\lambda d\lambda$ then the mean refraction is

$$\overline{R}=\tan z\frac{\int d\lambda\; n_\lambda R_0(\lambda)}{\int d\lambda\; n_\lambda} \tag{12}$$

and the dispersion is

$$\sigma^2_{\rm ref}=\overline{(R-\overline{R})^2}=\tan^2 z\frac{\int d\lambda\; n_\lambda (R_0(\lambda)-\overline{R}/\tan z)^2}{\int d\lambda\; n_\lambda}. \tag{13}$$

The dispersion is shown for various zenith angles is shown in table 5 for a box-car filter with upper cut-off at $\lambda=8500\mathring{A}$ and lower wavelength cut-off as indicated. The degradation in performance is given by $\sigma^2_{\rm ref}/(2\sigma^2_{\rm atm})$. At $z=70^\circ$ (air-mass $\simeq 3$) the degredation is about 20% at $\lambda_{\rm min}=5500$ and the degradation increases rapidly with decreasing $\lambda_{\rm min}$.

This calculation assumed a neutral (constant reflectivity) object and a realistic model for the detector quantum efficiency. This reduction in performance needs to be factored into the calculation of the optimal band-pass for asteroid detection (see below).

3.6 Telescope Aberration

Figures 6 and 6 show contour plots of the telescope PSF as calculated from diffraction theory by the ZEMAX program.

Table 6 shows the area of the PSF: $\sigma^2=\int d^2r\;(x^2+y^2)g(\mathbf{r})/2\int d^2r\; g(\mathbf{r})$ as a function of angle from the field center.

These results give an absolute lower bound on the performance for this design. Actual aberrations may be worse depending on e.g. collimation of the instrument.

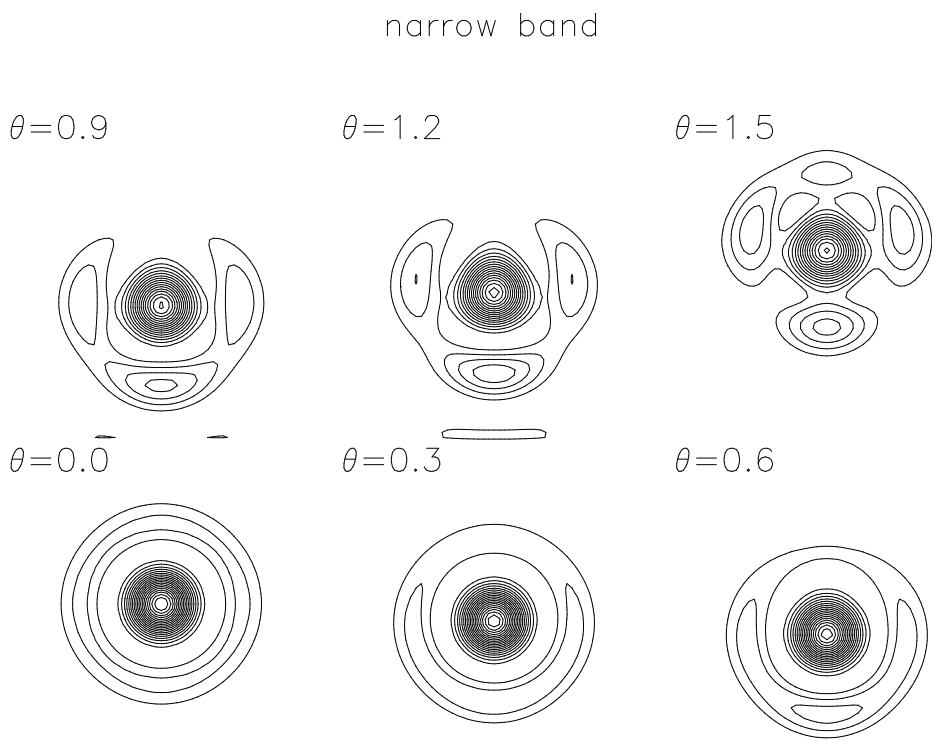

Figure 6: Telescope point spread function computed for design PS-3L-14 using diffraction theory. Focus was optimised for a narrow band at $\lambda = 7000\mathring{A}$. The labels indicate the distance from the field center in degrees.

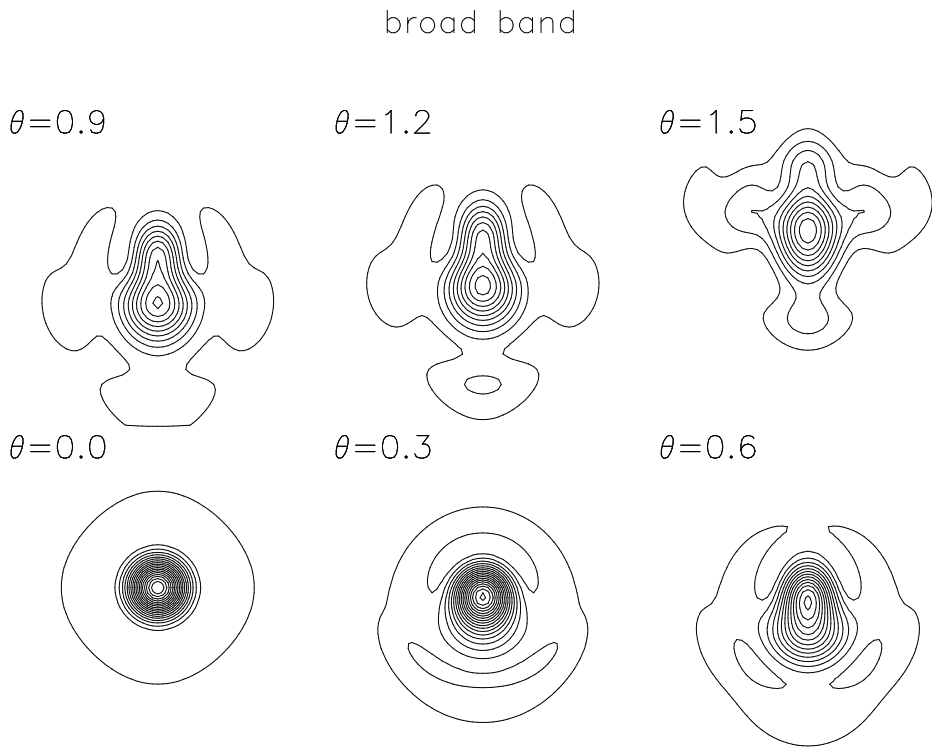

Figure 7: Telescope point spread function computed for design PS-3L-14 using diffraction theory. Focus was optimised for a broad band covering $5500\mathring{A} < \lambda = 11000\mathring{A}$.

θ	$\sigma^2(\lambda = 7000\mathring{A})$	$\sigma^2(5500\mathring{A} < \lambda < 11000\mathring{A})$
0	0.01331812	0.01543516
0.3	0.01322964	0.01552935
0.6	0.01313391	0.01591188
0.9	0.01382943	0.01684709
1.2	0.01337899	0.0161692
1.5	0.01277933	0.01547222

Table 6: Area of 'Huygens PSF' as calculated by ZEMAX for the design PS-3L-14.

4 Filter Design

Many science applications require color information, and this dictates the choice of filters. For asteroid detection, however, the color information is of little use, and one would like to use a filter that maximizes the signal-to-noise ratio. We show in §4.1 that, assuming one can design a filter of arbitrary transmission function, the optimum filter consists of a set of one or more 'box-cars' with unit transmission and with zero transmission at intervening wavelengths. The points on the spectrum where the transitions from zero to unit transmission occur are those wavelengths where the ratio of source counts to total (sky + source) counts is half the ratio of source to source + sky counts within the region where the transmission is unity.

This would lead, naturally enough, to a filter that notches out all the sky lines. Since that is impractical, we explore instead, and in §4.3, more practical (though still somewhat idealized) filters that are 100% transmissive between a minimum and maximum wavelength.

4.1 Optimal Filter Transmission Function

Let the object deliver on average, and for the given integration time, a mean number of electrons

$$\overline{N}_o = \int d\nu\, \overline{N}_o(\nu) W(\nu) \tag{14}$$

where $\overline{N}_o(\nu)d\nu$ is the mean number of electrons that would be created from the radiation in the range of frequency $d\nu$ around ν with no filter (i.e. it includes the system quantum efficiency), and $W(\nu)$ is the (energy) transmission function of the filter.

Similarly, let the sky deliver, on average, a number of electrons

$$\overline{N}_s = \int d\nu\, \overline{N}_s(\nu) W(\nu) \tag{15}$$

and denote the total counts by $\overline{N} = \overline{N}_o + \overline{N}_s$.

A fair estimator of the source counts is $\hat{N}_o = N - \overline{N}_s$ and the expected variance in this estimator is, from Poisson statistics, $\sigma^2_{\hat{N}_o} = \langle (\hat{N}_o - \overline{N}_o)^2 \rangle = \overline{N}$. The signal to noise ratio is then

$$\mathrm{SN} = \langle \hat{N}_o \rangle / \sigma_{\hat{N}_o} = \frac{\overline{N}_o}{\sqrt{\overline{N}}} = \frac{\int d\nu\, \overline{N}_o(\nu) W(\nu)}{\sqrt{\int d\nu\, \overline{N}(\nu) W(\nu)}} \tag{16}$$

where $\overline{N}(\nu) = \overline{N}_o(\nu) + \overline{N}_s(\nu)$.

If we differentiate with respect to $W(\lambda')$ to try to find a filter transmission function that renders the signal-to-noise stationary we obtain the equation

$$\frac{\overline{N}_o(\nu')}{\overline{N}(\nu')} = \frac{1}{2} \frac{\int d\nu\, n_o(\nu) W(\nu)}{\int d\nu\, n(\nu) W(\nu)}. \tag{17}$$

This must be true for all ν'. However, in general the left hand side depends on ν' while the right hand side is independent of ν', so this equation cannot be satisfied.

It follows that there is no transmission function $W(\nu)$ that renders the signal to noise *stationary*. The only way for the signal to noise to be *maximized* is for $W(\nu)$ to be driven to one of its physical limits, $W(\nu) = 0$ or $W(\nu) = 1$. The function $W(\nu)$ must be series of one or more box-cars. Requiring that the derivative of SN with respect to the limit $\nu_\star$ of one of these box-cars yields the equation

$$\frac{\overline{N}_o(\nu_\star)}{\overline{N}(\nu_\star)} = \frac{1}{2}\frac{\int d\nu\ n_o(\nu)W(\nu)}{\int d\nu\ n(\nu)W(\nu)} = \frac{1}{2}\frac{\overline{N}_o}{\overline{N}} \tag{18}$$

i.e. the ratio of the object to total counts at the margin is one half of the ratio of the mean total object to total object plus sky counts.

4.2 Dependence on Source Flux Density

For faint sources we can take $\overline{N} \simeq \overline{N}_s$ in (18), while for bright sources $\overline{N} \simeq \overline{N}_o$, and is is optimal to use no filter at all. The sky surface brightness is around 21mag per square arcsec in V and R bands, so, with ~ 1 arcsec seeing one might expect to be in the faint source regime for sources of greater than about 21st magnitude.

To make this a little more precise, note that the total electron count is

$$\overline{N} = \overline{N}_s + \overline{N}_o \propto f_s \int d^2x\ g(\mathbf{x}) + F_o \int d^2x\ g^2(\mathbf{x}) \tag{19}$$

where $g(\mathbf{x})$ is the PSF, $\mathbf{x}$ denotes angle, f_s is the surface brightness of the sky and F_o is the flux density of the object.

If we model the PSF as a Gaussian: $g(\mathbf{x}) = (2\pi\sigma^2)^{-1}\exp(-x^2/2\sigma^2)$ then $\int d^2x\ g^2(\mathbf{x}) = 1/4\pi\sigma^2$, and the ratio of mean object to mean total counts is

$$\frac{\overline{N}_o}{\overline{N}} = (1 + F_o/4\pi\sigma^2 f_s)^{-1} = \left(1 + \frac{2.35^2}{4\pi}\frac{F_o}{f_s \mathrm{FWHM}^2}\right)^{-1}. \tag{20}$$

Since Pan-STARRS will be able to detect sources of approximately 24th magnitude in $\sim$ 30s integrations, it should be quite safe to take $\overline{N} \simeq \overline{N}_s$.

4.3 Single Band Filter Optimization

The objects we are interested in (asteroids) have rather smooth SEDs, much like the sun, while the sky, particularly at red wavelengths is a mass of emission lines. Applying the above results literally would result in an optimal filter that consists of a set of notches to remove the sky lines while allowing signal through. This is probably impractical. Here we explore the efficiency for a simple broad-band filter, assumed to be fully transmissive for $\lambda_1 < \lambda < \lambda_2$ and non-transmissive otherwise.

In the POI Book efficiency calculations were performed for standard V, R filters and compared to a broader $V + R$ filter (the former two being similarly efficient for neutral colored objects, and the latter, consequently being roughly a factor 2 more efficient). Here we will show that the $V + R$ filter is about 60 percent as efficient as a broader filter.

To perform this calculation we need at least the following resources.

1. An object SED — we use the G2 (solar type) spectrum (#45 of Gunn and Stryker).
2. A dark sky spectrum — provided by Alan Stockton. Two spectra
3. A system quantum efficiency — we use the device QE measured by John Tonry. Ideally we would include mirror reflectivity, sky extinction etc, but these are relatively minor and so were ignored for simplicity.

The distribution of electrons generated over wavelength — the product of the distribution of photons (figure **??**) and the quantum efficiency (figure **??**) — is shown in 8.

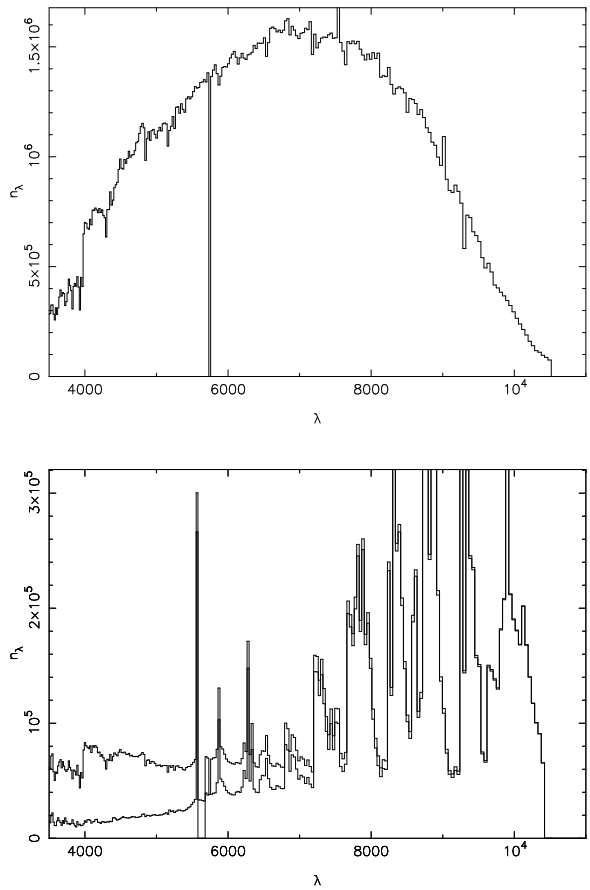

Figure 8: Distribution of electrons over wavelength for the sun (upper panel) and for the sky emission (lower panels).

The efficiency (the square of the signal to noise ratio given by (16)) computed according to the above formula for a simple box-car filter is shown in figure 9 for dark conditions and for half moon conditions.

A reasonable compromise between moon-less and moon-lit conditions would seem to be to have a wavelength range of about $4000-8000\mathring{A}$. However, as discussed in §subsec:efficiency:atmosphericrefraction, for observations at high air-mass, there is an efficiency loss from dispersion. Asteroids detected in the sweet-spots have larger velocities than those detected at opposition, typically around 1 degree per day. For 30s integration this gives a trail of length $1''.25$, and a reduction in efficiency of about 42%. This produces a dispersion (one dimensional) of $\sigma^2 = d^2/12 \simeq 1.3e \times 10^{-1}$ or equivalent to the effect of a filter extending to $\lambda_{\min} = 4500\mathring{A}$. For $\lambda_{\min} > 5000\mathring{A}$ the effect of the atmospheric refraction is relatively small.

5 Limits on Astrometric Precision

5.1 Measurement Error

For faint sources, the uncertainty in position is

$$\sigma_x^2 \simeq 0''.070(\mathrm{FWHM}/0''.6)/\nu. \tag{21}$$

For faint sources the fundamental limit from photon-counting statistics is

$$\sigma_x^2 \sim (\mathrm{FWHM}/2)^2/N_s \tag{22}$$

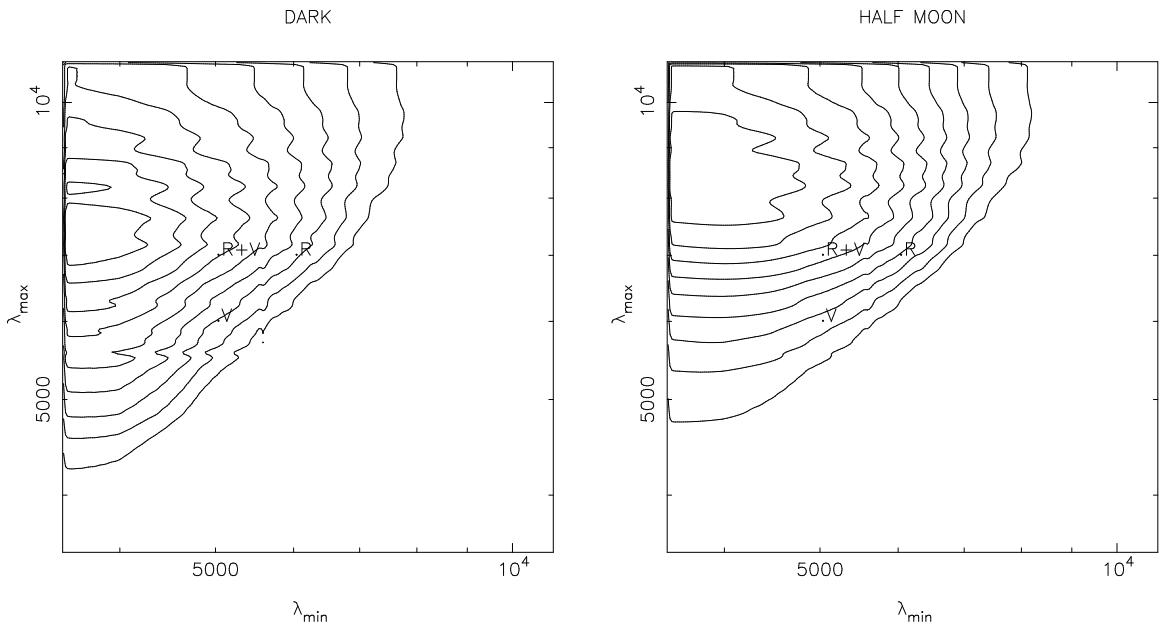

Figure 9: Efficiency as a function of the wavelength cut-offs for a simple box-car filter. The contours shown are equally spaced between 10% and 90%. Also shown are the standard V and R broad-band filters and also for a $V + R$ filter. The highest efficiency is at upper left, with upper cut off around $\lambda_{\rm max} \simeq 7300\mathring{A}$ and a lower cut-off at at most $\lambda_{\rm min} \simeq 4000\mathring{A}$. However, this calculation does not include differential refraction, which may dictate a longer wavelength cut-off.

with N_s the number of electrons from the source.

5.2 Systematic Errors

It is relatively straightforward to link the Pan-STARRS astrometric system to a dense external catalog like USNO-B. Experience shows that it is possible to achieve ~ 5 milli-arcsec precision for relative astrometry — i.e. the objects line up to this level of precision. However, the system would inherit any systematic errors in the external catalog. These are thought to be at the $\sim 0''.1 - 0''.2$ level, considerably larger than the measurement error even for faint sources.

With more work it should be possible to measure and then correct for these systematic errors. One application that would benefit from this is asteroid detection. A favored approach for asteroid hunting is to link observations on several nights with an interval of 3-4 nights (and with at least one multiple observation with a base-line of an hour or thereabouts to confirm the linkage). With motions of the order of a degree a day, we are talking about a ~ 10 degree arc. The smaller we can make the uncertainty, the smaller the future error ellipsoid and the easier it is to establish linkage with future observations.

However, the process of identifying systematics in the external catalog may be limited in practice by atmospheric refraction fluctuations. The hope is that if one can understand and model the behaviour of the telescope and detector then one can detect anomalies in the distortion mapping that are due to errors in the external catalog. Using overlapping observations one can confirm that the anomaly is really fixed on the sky. Unfortunately, the standard theory of atmospheric turbulence predicts random fluctuations in the distortion that produce deflections coherent over large angles and that average out slowly with time, making it hard to determine the external systematic errors. It is thought that the atmosphere is limiting the Pan-STARRS, 2MASS precision to the $\sim$ 50mas level.

The RMS $\sigma_{\rm def}$ of the instantaneous tilt wavefront from a turbulent layer, averaged over a disk of

diameter D, is

$$\sigma_{\rm def} \simeq 1.0 \frac{\rm FWHM}{2.35} \left(\frac{D}{r_0}\right)^{-1/6} \tag{23}$$

with r_0 the Fried length (the width of the seeing disk being FWHM $\simeq 1.0\lambda/r_0$). Averaged over an integration time $t_{\rm int}$, the deflection averaged over a disk of angular diameter $\theta = D/h$ is

$$\sigma(\theta, t_{\rm int}) \simeq \frac{\rm FWHM}{2.35} \left(\frac{h\theta}{r_0}\right)^{-1/6} \left(\frac{v t_{\rm int}}{h\theta}\right)^{-1/2} \propto \theta^{1/3} t^{-1/2} \tag{24}$$

Kolmogorov theory predicts deflections growing with angular scale. More realistically we would expect this growth to be cut off at the outer scale L_o. Allowing for this the 1-sigma precision from the atmosphere can be written as

$$\sigma_x \simeq 0''.16 \left(\frac{\rm FWHM}{0''.6}\right)^{5/6} \left(\frac{L_{\rm o}}{20{\rm m}}\right)^{1/3} \left(\frac{v}{10{\rm m/s}}\right)^{-1/2} \left(\frac{\lambda}{5\times10^{-7}{\rm m}}\right)^{1/6} \left(\frac{t_{\rm exp}}{1{\rm s}}\right)^{-1/2}. \tag{25}$$

The time-scale for variation of deflections on this scale is

$$\tau \simeq \frac{L_{\rm o}}{v} = 2{\rm s} \left(\frac{L_{\rm o}}{20{\rm m}}\right) \left(\frac{v}{10{\rm m/s}}\right)^{-1}. \tag{26}$$

The angular scale on which these deflections occur is

$$\theta \simeq L_{\rm o}/H \simeq 12' \frac{L_{\rm o}}{20{\rm m}} \frac{5{\rm km}}{H} \tag{27}$$

where H is the height of the layer. For very low altitude turbulence the angular scale may be stretched to be larger than the field of view, effectively reducing the amplitude of the deflections within the field.

The first three factors in (25) are determined by the environment. The only factor under the control of the observer is the integration time. The only way to achieve absolute astrometric accuracy is to integrate sufficiently long to average out the large-scale atmospheric deflections.

For the fiducial parameters chosen (the standard assumptions used in e.g. analysis of MCAO systems), equation (25) does not account for the systematics found in the SDSS analysis, but it would if we were to take an outer-scale of 300m and typical seeing of FWHM = $1''.5$ we would obtain $\sigma_x \simeq 50$mas as found empirically.

Another useful empirical input comes from analysis of Tonry's measurement of relative motions of guide stars with separations $\sim 10'-15'$. Averaged over time of 30s, the rms relative deflection is often around 10mas or lower, considerably less than (25) would suggest. The rigidity of the pattern of stars in Tonry's measurements are good news, and suggest that, on Mauna Kea, atmospheric limitations on astrometry precision will not be a serious problem. Seeing is a stochastic phenomenon, so care should be taken in the pre-survey to ensure that all of the survey region is observed under good conditions.

6 Image Processing Pipeline

The task of the image processing pipeline is to generate, in some pixellated form, a set of images of patches of the sky projected onto a set of tangent planes (see figure 10)

If we assume that the sky is static; that the statistics of the fluctuations in the pixel values due to atmospheric emission and read-noise are Gaussian; and that the source surface brightness (after convolution with the system PSF) is low compared to the sky then the likelihood of the image scene is a function of a single image. This image is constructed by laying down for each pixel, at the point on the sky that maps to the center of the pixel, a copy of the point spread function with weight proportional to the excess count, over that of the sky, for the pixel.

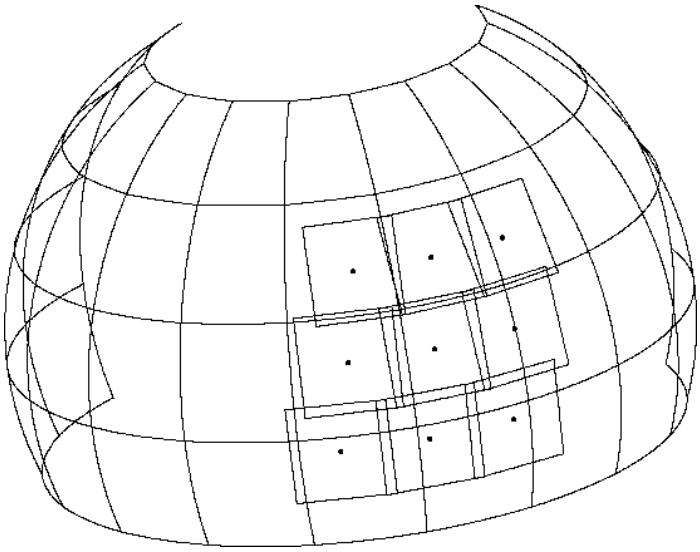

Figure 10: Pan-STARRS will observe a set of fields around the sky. The data products will be generated as projections of the sky surface brightness onto tangent planes, as shown grossly exagerrated above.

Combining the images in this way preserves all of the information in all of the source images that is of any relevance to studies of faint objects of any kind. This answers the often posed question as to how Pan-STARRS will cope with variable image quality. In this algorithm all of the data are combined with optimal weight. The idealised model from which the optimal combination algorithm derives suffers from two minor problems: First, the sky is not really static, so one would want e.g. to remove bright satellite trails. Second, the pixel noise is not precisely Gaussian, but for Pan-STARRS it is a very good approximation for all relevant integration times. There are two more serious problems:

1. The combined image is a continuous function, and is therefore not computable. One should think of the optimal algorithm as being a limiting case, against which one can assess the performance of any practical implementation that would have finite sampling. The performance of the implementation can therefore be measured by how well the results approximate the infinite resolution limit.

2. Some of the image data will suffer from patchy extinction, and, depending on the spatial frequency, it may be hard to correct for. For some applications this is benign, but not for others. This needs more study via simulations, but may dictate construction of a separate accululated image using a subset of data for applications that require exquisite photometric accuracy.